Journal of Lasers in Medical Sciences

J Lasers Med Sci 2021;12:e89

Original Article

http://journals.sbmu.ac.ir/jlms

doi 10.34172/jlms.2021.89

Developing a New Dimension for Fourier Domain Optical Coherence Tomography Images by Simultaneous Measurement of the Refractive Index and Thickness

Ahmad Amjadi[1,*], Hamed Ghodsi[2], Salile Khandani[2], Bahareh Khishkhah[2], Payman Rajai[2], Mohammadreza Razzaghi[1]

[1]Laser Application in Medical Sciences Research, Shahid Beheshti University of Medical Sciences, Tehran, Iran
[2]Sharif Applied Physics Research Center, Physics Department, Sharif University of Technology, Tehran, Iran

***Correspondence to**
Ahmad Amjadi,
Email: amjadi@sharif.edu

Received: September 3, 2021
Accepted: December 1, 2021
Published online December 29, 2021

Abstract

Introduction: Fourier domain Optical coherence tomography (OCT) is a widely used high-resolution optical imaging technique. It is useful for various applications in medical imaging, such as ophthalmology (e.g. retinal imaging for diagnosing complications like glaucoma or macular degeneration), dermatology, oncology, and cardiology. The ability to noninvasively measure both the refractive index and thickness of biological tissues could have various medical applications and enable earlier disease detection. For example, observing changes in the refractive index can help distinguish between tissues with normal or abnormal function.

Methods: In this study, the theoretical framework for simultaneous measurement of the refractive index and physical thickness of multilayer systems is proposed and tested for two different samples, each having three layers, a glass/NaCl solution/glass sample and a glass/sugar solution/glass sample. The whole signal processing procedure and the experimental setup are described.

Results: The refractive index and thickness of salt water and sugar water samples in the Fourier-domain OCT (FD-OCT) system were obtained. The resulting data were compared with reference measurements and showed a deviation of about 1% for the samples.

Conclusion: We tested the proposed framework for the simultaneous extraction of the refractive index and thickness of multilayer systems of salt water and sugar water from its FD-OCT data. We showed that the measured parameters were in agreement with reference amounts.

Keywords: Optical coherence tomography; Refractive index; Fourier domain OCT; Medical imaging; Ophthalmology.

Introduction

Throughout the last two decades, optical coherence tomography (OCT) has become an established technique in numerous research domains as a noninvasive cross-sectional imaging tool.[1] Although the main application of OCT is in ophthalmology, there is emerging attention to the employment of OCT techniques in other medical and industrial applications[1] such as diagnosing and screening neural diseases like Alzheimer, Parkinson and multiple scoliosis (MS),[2] OCT-based cardiovascular imaging[3] and the assessment of cancers like brain tumors, breast cancer, and melanoma.[4-7] Therefore, improving OCT imaging techniques and developing related applications have become the subject of many research articles. Among them, quantum OCT,[8] polarization-sensitive OCT,[9] and simultaneous measurement of thickness and refractive index[10] are some of the most effective propositions.

In this paper, a method for extracting the refractive index from the measured optical path length has been implemented, experimentally investigated, and characterized as an extra dimension or extra level of precession to the resulting information. The authors believe the extraction of this information is essential for two reasons. First, reporting the physical thickness of layers is important since many medical indications are based on the thickness of specific layers.[11] Secondly, this potential can be seen as a powerful diagnostic tool in medical applications like finding tumors with different refractive indexes from the normal tissue. Yun et al developed a method to measure both the refractive index and thickness from an OCT image.[11] The proposed technique is based on inserting a needle into the sample. Hence, this method is intrusive and is appropriate only for in vitro applications. However, for an in vivo application like retinal layers of a patient, this method cannot be used and the theoretical method proposed by[12] seems more

Please cite this article as follows: Amjadi A, Ghodsi H, Khandani S, Khishkhah B, Rajai P, Razzaghi M. Developing a new dimension for fourier domain optical coherence tomography images by simultaneous measurement of the refractive index and thickness. *J Lasers Med Sci.* 2021;12:e89. doi:10.34172/jlms.2021.89.

beneficial due to its non-invasive nature.

This paper discusses the implementation procedure and theoretical aspects in Materials and Methods section. In section (3), the experimental setup and composition of the test samples can be found, and in section (4), the results of our measurements are compared with the reference values and computer simulations.

Materials and Methods

The development of Fourier-domain OCT (FD-OCT) has provided notable improvements in the imaging rate and detection sensitivity.[13-16] Both spectrometer-based spectral-domain (SD-OCT) and swept-source OCT (SS-OCT) realizations are similar from a theoretical point of view because the measured spectrum discretized by the CCD pixels can be interpreted the same as the time-multiplexed output of the balanced detector in SS-OCT configuration.[12,17,18]The method used in this work and the experimental results are based on SD-OCT configuration, but a similar approach can be utilized for SS-OCT devices.

The SD-OCT system uses a broad-spectrum source similar to time domain (TD-OCT) systems. The main difference is the reference mirror does not move while scanning, which gives the system a far faster operating capability, and the balance detector is replaced by a system of diffraction gratings and a line scan camera.

In this paper, a summation method has been used for the calculations. This method requires a minor change in refractive indices in a sample in such a way that the multiple reflections are negligible.

As depicted in Figure 1, the field amplitude of the beam from a short coherent light source is divided into two parts by a beam splitter, one incident on a reference mirror and the other part incident on the object.

The total field at the beam splitter position is the sum of the fields reflected from each interface of the sample[9]:

$$E_s = \left(E_0^s + E_1^s + E_2^s + \cdots\right) = s(k)\sum_{j=0}^{N} r_j \exp(i2kZ_j) = s(k)\sum_{j=0}^{N} r_j \exp(i2k\sum_{l=0}^{j} n_l d_l) \tag{1}$$

where N is the number of layers of the object, k is the wavenumber in free space, n_l and d_l are the refractive indices and the physical thickness of the first layer ($n_0 d_0 = Z_0$), and $r_{(j)}$ is the reflected field amplitude from each interface.

The interference signal recorded on the detector is[18]:

$$\begin{aligned} I_{sum}(k) &= \left\langle \left|E_r + E_s\right|^2 \right\rangle = \left\langle \left(E_r + E_S\right)\left(E_r + E_S\right)^* \right\rangle \\ &= S(k)\left\{\left|r_R\right|^2 + \sum_{j=0}^{N}\left|r_j\right|^2\right\} \\ &+ 2S(k)\left\{\sum_{j=0}^{N} r_R r_j \cos\left[2k\left(z_R - z_j\right)\right]\right\} \\ &+ 2S(k)\left\{\sum_{n\neq m=0}^{N} r_n r_m \cos\left[2k\left(z_m - z_n\right)\right]\right\} \end{aligned} \tag{2}$$

Equation (2) consists of 3 parts:

- DC term which is independent of the path.
- CC term that is related to the optical path difference between the reflected beam from each interface and the beam reflected from the reference mirror.
- AC term caused by the interference between the reflected fields from different layers of the sample with each other.

The overall process of estimating refractive indexes from the spectral information can be described as shown in Figure 2. The first step is to resample the non-linear λ-sampled spectrum to linearly spaced data. Then the spectrum is filtered using a wavelet-based denoising filter and eventually using an iterative phase compensation algorithm[21,22]; existing nonlinearities and instrument dispersion effects are removed and the spectral data of a depth scan is ready for extracting the refractive indexes.

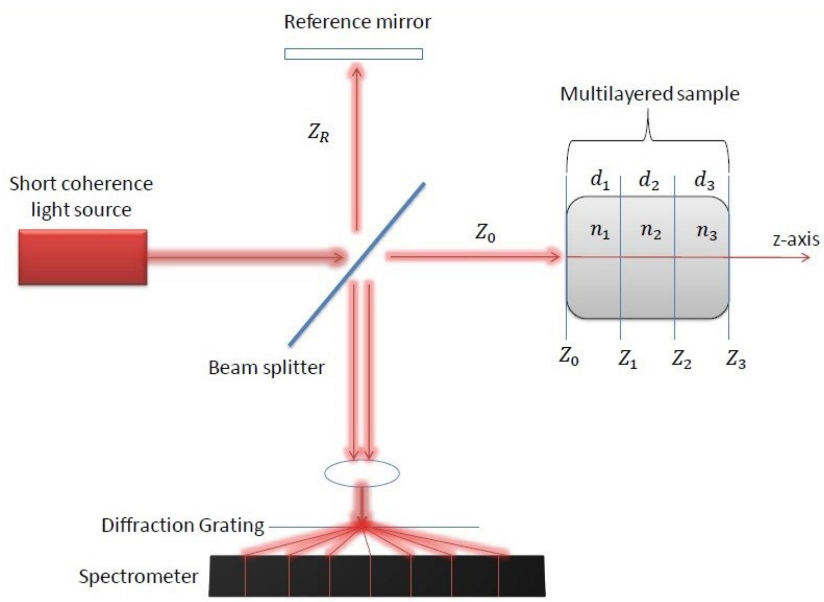

Figure 1. Schematic Presentation of the FD-OCT System.

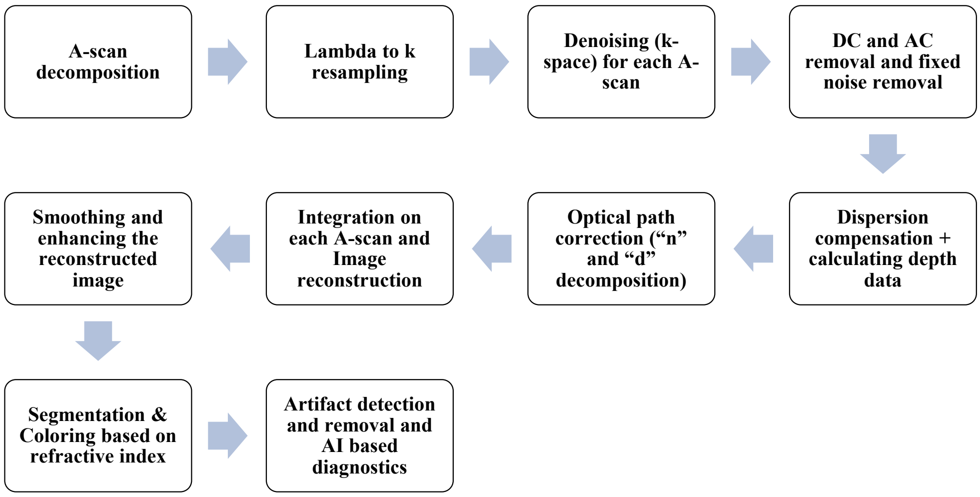

Figure 2. Workflow of the Refractive Index and Thickness Extraction.

Signal Processing

The procedure of manipulating the raw spectral data to be ready for refractive index extraction includes several steps. The first step is wave-number resampling. In many cases, spectrometer pixels are linearly spaced in the wavelength space which leads to non-linear sampled data in the wave-number space (wave-number = 2π/wavelength). This non-linear effect causes a depth-dependent broadening of depth-related peaks and therefore decreases OCT resolution. The simplest way is linear or cubic spline interpolation techniques, both of which result in considerable levels of resampling nonlinearity and depth-dependent dispersion.[23,24] Zero-padding interpolation is also an option with a lower non-linearity level and requires lower computing capacity.[25,26] In this paper, the zero-padding resampling method has been exploited. The performance of these methods is compared for a 1024-point measured raw interferogram of a multilayer scotch tape in Figure 3.

According to Figure 3c, linear interpolation considerably degrades the peak intensity and despite its lower execution time in MATLAB (about 9 ms) has not been used in this work. Although, spline interpolation and zero padding are comparable in terms of preserving the original peak intensity much less execution time for zero padding makes it beneficial to a high speed nature of OCT systems. According to our MATLAB algorithm spline interpolation took 44 ms for this single interferogram while zero padding by the factor of 3 using Fourier domain method (Figure 3c) needed about 10 ms.

After resampling, the k-space spectrum should be denoised using appropriate filters. There are many sources of noise contributing to SD-OCT systems, such as vibrational noise, fixed noise, electronic noise, and various detector noise.[27,28] Due to the high level of scattering and depth-dependent sensitivity limitations in SD-OCT systems, it is quite critical to decrease the signal to noise ratio (SNR) ratio as much as possible to reach the theoretically achievable depth. In our approach, denoising is done in several steps. The first step is a general denoising procedure consisting of low-pass and then wavelet-based filtering. Low-pass filtering should be done to remove the unwanted high-frequency spikes in the spectrum, and its cut-off frequency should be chosen above the highest meaningful frequency resulting from an interface placed in the maximum achievable depth. However, after low-pass filtering, the noise level is still high due to the existing noise in the same bandwidth as the signal. To reduce the effect of unwanted interferences and noises from the interferogram, wavelet-based denoising is proven fruitful.[11] Wavelet-based filters decompose the signal using several base functions and use soft or hard thresholding methods for denoising. In our case the filter design parameters such as filter order and thresholding method should be optimized for the interferogram signal for best performance and precision. To do so, we have examined several denoising methods like Bayesian[29-30] and James-Stein block wavelet-based thresholding[31] schemes. As a result, Daubechies wavelet basis and Stein thresholding method have been chosen for denoising the interferogram. and the result is shown in Figure 4 for the same interferogram as before. It should be noticed that due to the high scan rates in the SD-OCT devices, computational delay in each step is a key parameter in providing real-time high-quality results and wavelet-based denoising fulfills this requirement with a 20 milliseconds computational time in the MATLAB platform.

Fixed noises, high-intensity peaks at z = 0 (DC) and the unwanted autocorrelation (AC) peaks should also be removed for achieving a correct OCT tomogram. DC peak is easy to remove because its position is fixed and one just needs to find the first zero of the z-space results and put away everything before. Alternatively,

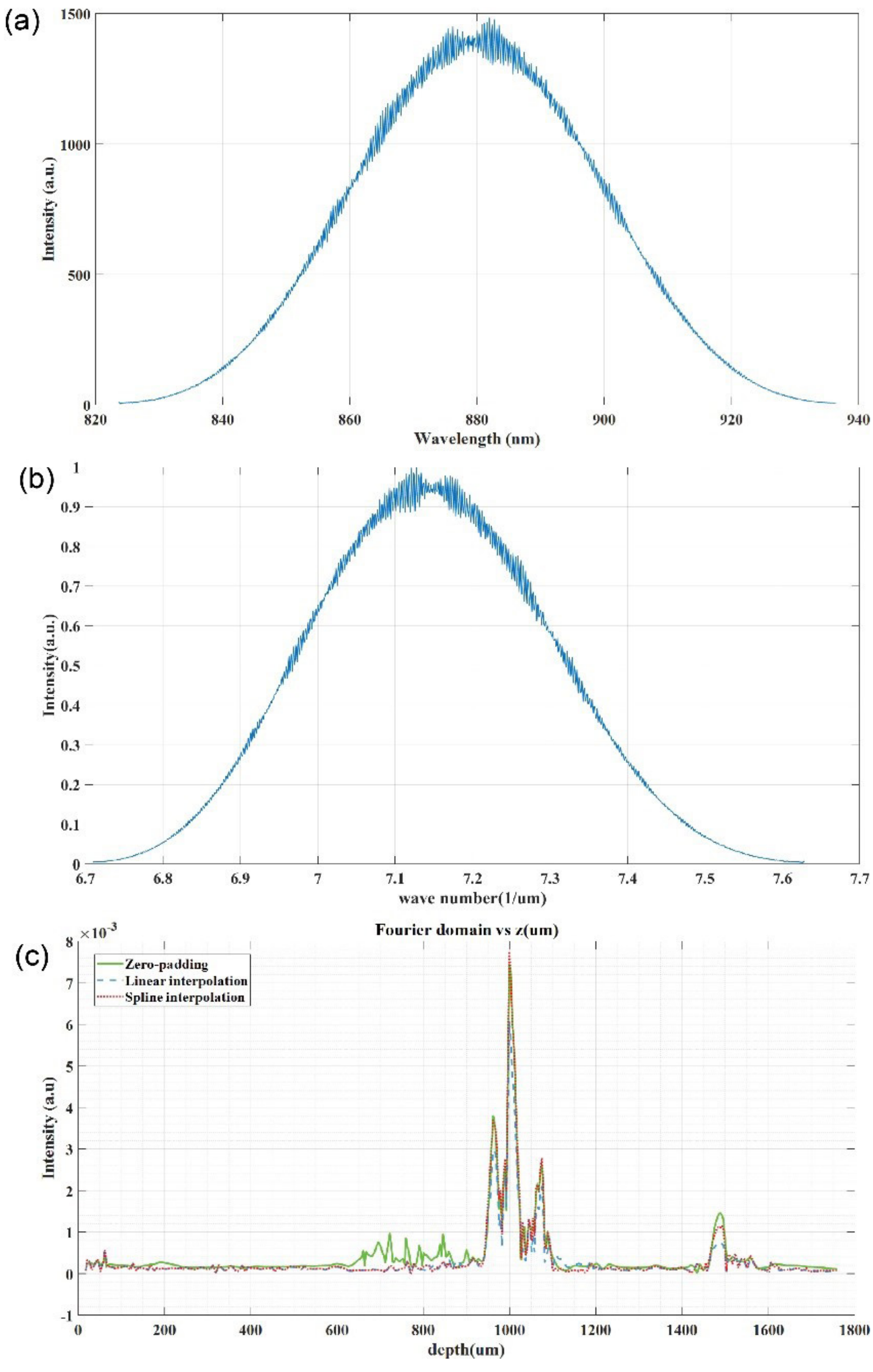

Figure 3. (**a**) Measured Interferogram, (**b**) Resampled k-Space Spectrum, and (**c**) Depth Domain Signal for Linear Interpolation (Dashed Line), Spline Interpolation (Dotted Line), and Zero-Padding (Solid Line).

it can be omitted by an appropriate high path filter on the spectrum. Autocorrelation peaks are related to the interference patterns resulting from the multiple reflections in the sample. However, autocorrelation peaks are more challenging to remove and methods like phase-shifting interferometry may be needed.[32] To keep the OCT setup hardware as simple as possible and due to the negligible effect of autocorrelation terms, we will neglect the autocorrelation noise for now and move to the next step.

Refractive Index Estimation

In this section, our method for decoupling refractive index and layer thickness will be described based on the mentioned processing algorithms and the summation method. For the sake of simplicity, a two-layer sample is assumed for the mathematical solution. However, it is safe to say that this method could be applied to samples with any number of layers while the summation method

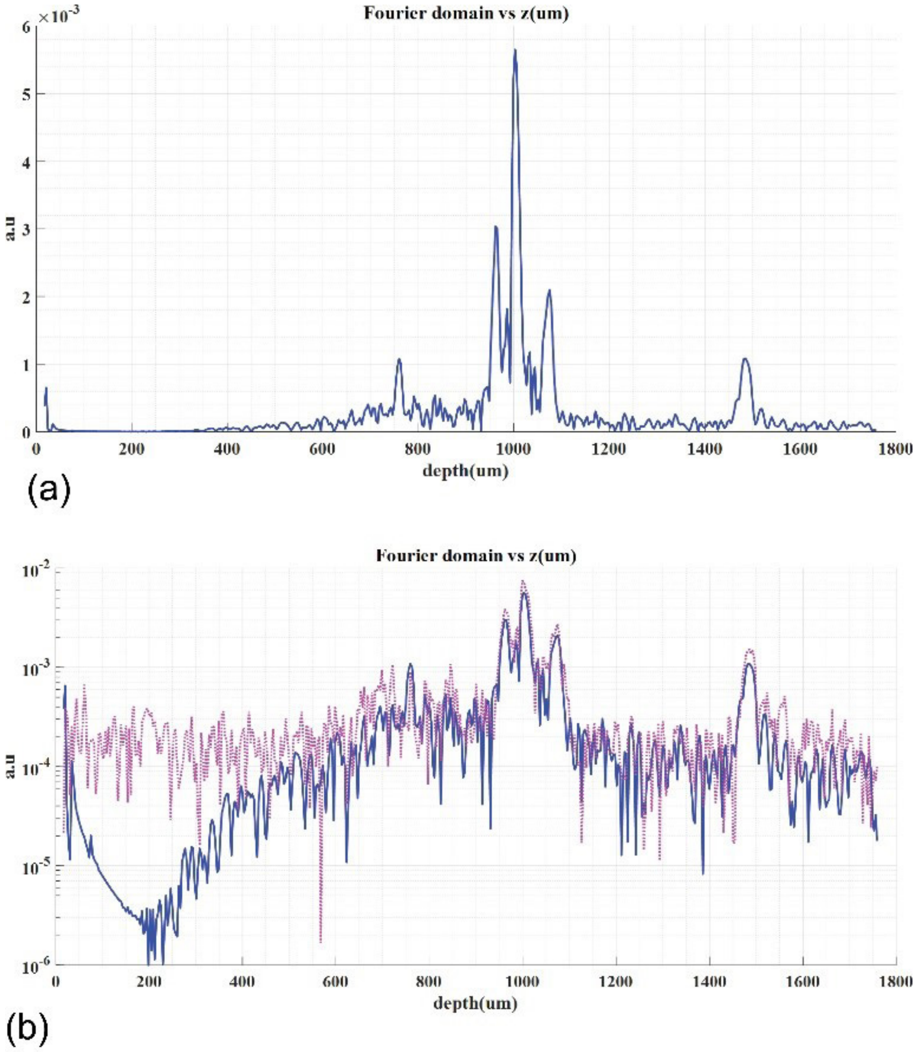

Figure 4. (a) the Denoised Depth Data of Figure 1, **(b)** Logarithmic Scale Result for Denoised Interferogram. solid line shows the denoised signal and dotted line illustrates the original noisy data.

assumption is preserved. Considering the two-layer system, the normalized signal after removing AC and DC terms is equal to[18]:

$$I_{SUM}(k) = \frac{I_{sum} - DC - AC}{2S(k)} \tag{3}$$
$$= r_1 \cos\left[2k\left(\Delta_{rz0}\right)\right] + r_2 \cos\left[2k\left(\Delta_{rz0} - \delta_1\right)\right] + r_3 \cos\left[2k\left(\Delta_{rz0} - \delta_1 - \delta_2\right)\right]$$

Where r_1, r_2, and r_3 are Fresnel reflection coefficients.

In this approach, we calculate the optical path length of each layer (δ1; δ2), which is the typical output of a conventional SD-OCT setup. These could be obtained from the Fourier transform of the interference spectrum. Considering (3) and having optical path lengths measured, there are three unknown reflection coefficients. As a result, we should choose three wavenumbers (k_1, k_2,k_3) to solve for these three values which lead to (4). These three points in the wavenumber space should be precisely selected to minimize calculation error originating from any approximation in the summation method One can do this by recursively sweeping the whole spectrum for a combination with minimized error for a test sample with a known refractive index and thickness.

$$\begin{bmatrix} r_1 \\ r_2 \\ r_3 \end{bmatrix} = P^{-1}. \begin{bmatrix} I(k_1) \\ I(k_2) \\ I(k_3) \end{bmatrix} \tag{4}$$

Where,

$$P = \begin{bmatrix} \cos\left[2k_1\left(\Delta_{rz0}\right)\right] & \cos\left[2k_1\left(\Delta_{rz0}-\delta_1\right)\right] & \cos\left[2k_1\left(\Delta_{rz0}-\delta_1-\delta_2\right)\right] \\ \cos\left[2k_2\left(\Delta_{rz0}\right)\right] & \cos\left[2k_2\left(\Delta_{rz0}-\delta_1\right)\right] & \cos\left[2k_2\left(\Delta_{rz0}-\delta_1-\delta_2\right)\right] \\ \cos\left[2k_3\left(\Delta_{rz0}\right)\right] & \cos\left[2k_3\left(\Delta_{rz0}-\delta_1\right)\right] & \cos\left[2k_3\left(\Delta_{rz0}-\delta_1-\delta_2\right)\right] \end{bmatrix} \tag{5}$$

After solving the equation for the Fresnel coefficients, assuming n_0 is known, the refractive indexes can be calculated from Fresnel coefficients:

$$r_1 = \frac{n_0 - n_1}{n_0 + n_1}, r_2 = \frac{n_1 - n_2}{n_1 - n_2}, r_3 = \frac{n_2 - n_3}{n_2 + n_3} \tag{6}$$

Accordingly, the thickness of each layer can be obtained from:

$$d_{1,2} = \frac{\delta_{1,2}}{n_{1,2}} \quad (7)$$

As mentioned before, this method can be generalized for a system of many layers as long as the summation approximation is valid. Moreover, beyond the summation approximation, the resulting set of equations that will be more complex and intermixed can still be solved and this method can be applied for noninvasive measurement of the refractive index of layers in a variety of samples.

Image Reconstruction

The previous section explored the method to calculate the refractive index in a simple A-scan. In this section, image reconstruction for a complete image comprised of several A-scans will be shortly discussed and the possible benefits will be explained.

According to section 2.2, the refractive index and thickness of each layer can be calculated using the summation method. By repeating this process for every A-scan, one can build a matrix in which every interface is marked by 1 and the rest zero. The resulting image is a black and white image that can show the dimensions correctly rather than showing approximately optical paths. The next steps are to color the image with a colormap corresponding to the changes in the refractive index for each layer and apply suitable image processing algorithms to reach more realistic or more favorable results based on the user's needs. As mentioned in the introduction, generating a refractive index depth map of the sample under test can be beneficial in many circumstances.[31,32]

Experimental Setup

A schematic of the setup is depicted in Figure 5. It consists of a white LED as the light source, a pinhole with a 500 nm diameter and two lenses to make a narrow parallel beam. The beam is aligned to have the narrowest diameter at the sample position.

The beam splitter should be perpendicular to the incident beam, the reference mirror is also placed perpendicular to the incident beam on a micrometer rail, the length of the sample and reference arms are equal and the sample surface is perpendicular to the beam to overlap more efficiently. Thin layers of saturated salt-water and sugar-water solutions at room temperature are used as the samples in our experiment.

- Two S1 lamellas with a thin layer of salt water in between (saturated at room temperature).
- Two S1 lamellas with a thin layer of sugar water in between (saturated at room temperature).

After installation of the setup for each sample, the reference mirror is moved on the rail with micrometer accuracy so that its reflection is at a suitable distance (less than the source coherence length). To observe the peak of the layers (after taking the Fourier transform) with the highest height, it was tried to minimize the difference between the lengths of the two arms for the mirror and the first border of the sample, so the first peak is created almost at the origin. This goal was achieved by moving the mirror to achieve the lowest frequency interference outside the sample range.

The specifications of the spectrometer are presented in Table 1.

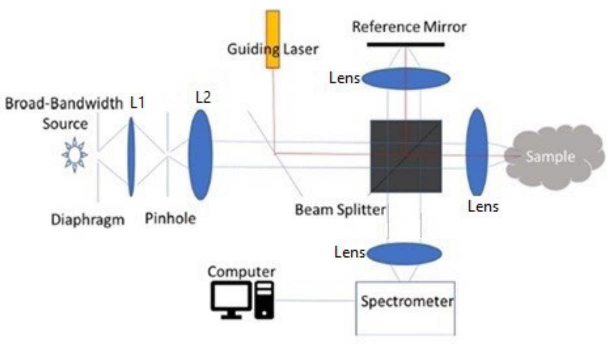

Figure 5. The Schematic of the Spectral Domain-OCT Setup .

Results and Discussion

The results of experiments on saltwater and sugar water are presented in this section.

The spectrum shown in Figure 6 is linearized by combining zero padding and linear interpolation methods, and noise correction is performed by correcting the wavelet coefficients. In Figure 5, using the Hilbert conversion method and also eliminating the scattering effects, the depth domain data scattering effects are depicted. Also, for more clarity, the first peak due to the border behind the lamen glass is removed and the two peaks shown in Figure 7 are related to the border between the first lamen glass and saltwater and the second lamen glass and saltwater. In this figure, the distance between

Table 1. Spectrometer Information

CCD sensor	Toshiba TCD 1304AP
Optical bench	Czerny turner
Measuring range	200-1100 nm
Resolution	1.8 nm
Slit	25 um
Pixel	3648
pixel size	8 um * 200 um
pixel depth	100 000 electrons
Signal to noise ratio	800:1
Exposure time	10 us –60 s
A/D resolution	16 bit
Linear variable filter	Yes
Weight	430 g
Dimensions	102 mm * 84 mm * 59 mm
Fiber optic connector SMA (um)	SMA905 (400 um)
External trigger	Yes

them represents the light length (the product of the refractive index of water and salt and the thickness of the saltwater layer).

In the second image, the distance between the two peaks is equal to 10.5 μm. If we use the algorithm designed in the previous sections to separate the refractive index and thickness, for this example, we will reach the actual thickness of 7.95 microns and the refractive index of 1.32.

To measure the accuracy of this method in a real trial, a standard sample with certain specifications must be used according to the measurement limitations of the set-up, so that we can test the accuracy of this method correctly. In this regard, using the refractometer, we measured the refractive index value of this sample accurately, which was 1.3335, indicating a very small error of refractive index measurement of 1%.

For examining the accuracy of this method and overcoming the limitations of the set-up made for use in Figures 6 and 7, another sample is prepared with a solution of water and sugar, which is expected to have a different refractive index than the water and salt sample. In this example, the optical length of the water and sugar layer is 13 microns, and according to the described algorithm, the refractive index and the actual thickness of this layer can be obtained as 1.35 and 9.63 microns respectively. These data were obtained for an A-scan in-depth scan. The measured refractive index for this sample was 1.3375 using the refractive index, which again shows a similar error of 1%. A real and practical sample, for example, ophthalmology, requires more research.

Figure 8 shows the interference spectrum of the lamellar sample with the water and salt layer, acquired by the set-up used in this study. The white light spectrum of the LED source is also intended for the light source. As it is shown, the spectral width of this light source is very large, which theoretically creates a very small coherence length, resulting in high resolution at depth.

In Figures 7 and 9, the refractive index of each of the water-salt and water-sugar samples according to the length of the sample, which in the first lamel consists of glass and water-salt and glass and in the second lamel consists of glass and water-sugar and the glass is drawn.

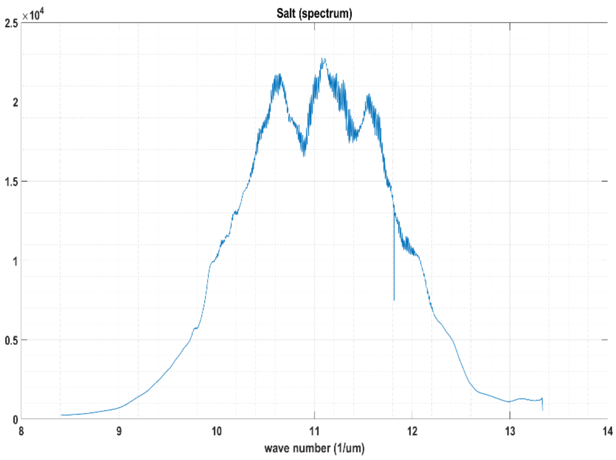

Figure 6. Processed Spectrum for Saltwater Sample.

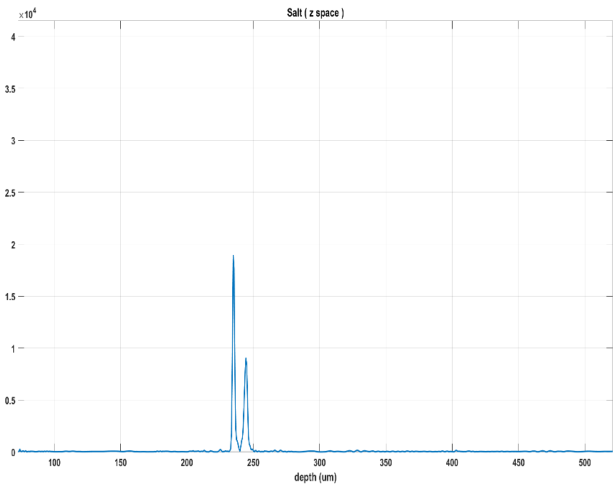

Figure 7. Fourier Transform Image for a Saltwater Sample.

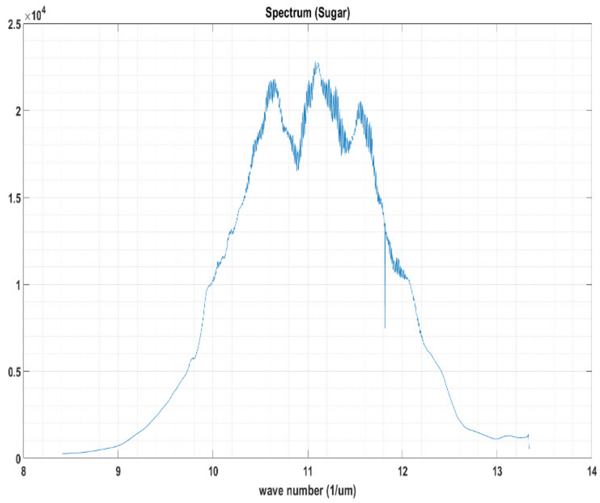

Figure 8. Spectrometer spectrum image for sugar water sample.

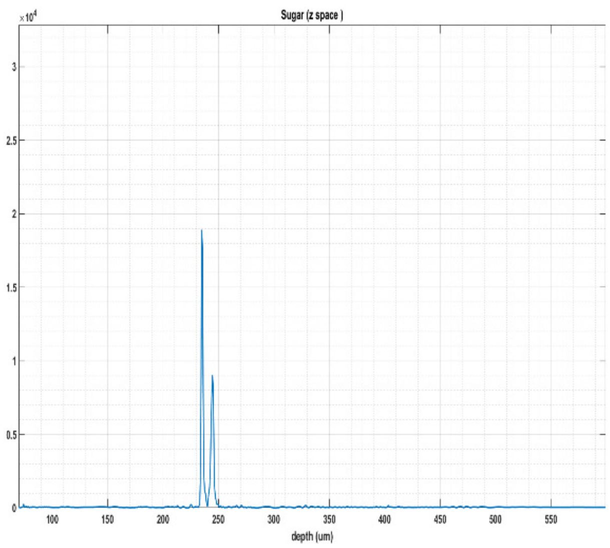

Figure 9. Fourier Transform Image for a Sample of Sugar Water.

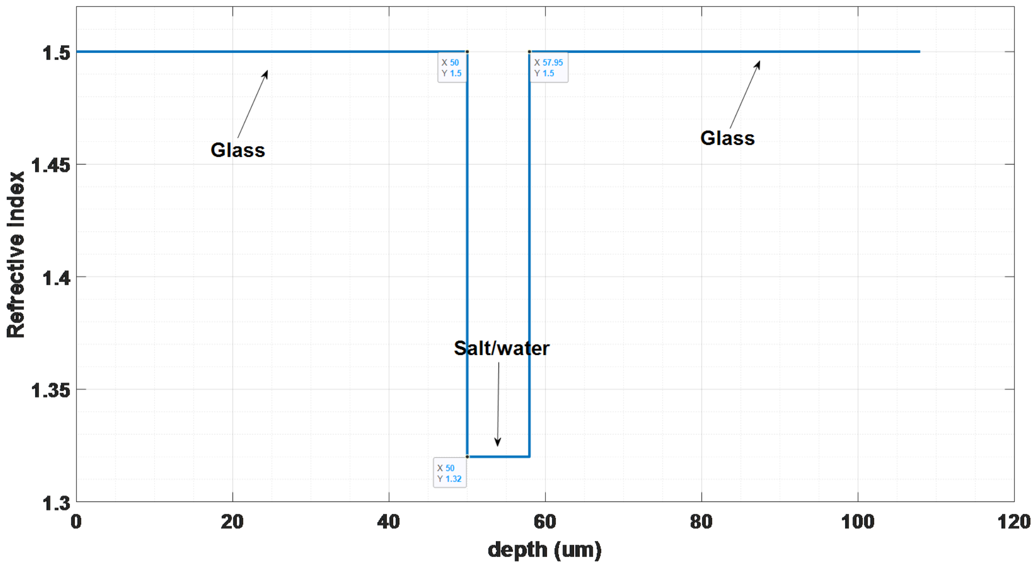

Figure 10. Diagram of Refractive Index Changes in Terms of Sample Length for the Salted Water .

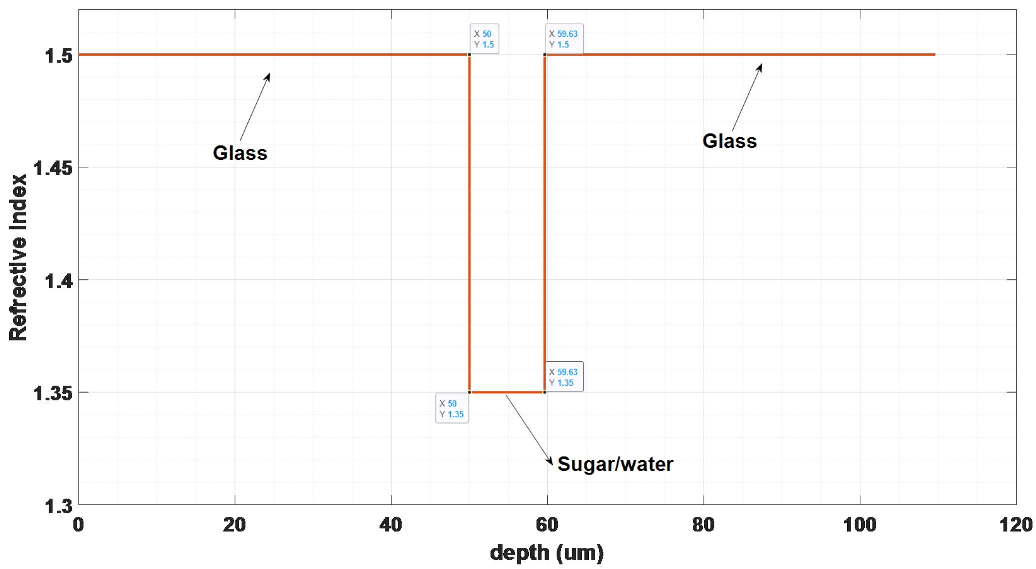

Figure 11. Diagram of Refractive Index Changes in Terms of Sample Length for the Sugar Solution.

Figure 10 and 11 show the refractive index changes in terms of sample lengths for salted water and sugar solution, respectively.

Conclusion

As mentioned before, existing methods and devices are not able to measure the thickness and refractive index separately for the sample. In this project, using the theory that we introduced for simultaneous measurement of the physical thickness and refractive index of multilayer systems, we were able to simultaneously measure the refractive index (n) and physical thickness (d) for the test samples (salt water and sugar water) and validate the results. We want the sample (same information) as FD-OCT, which is used to calculate the optical thickness of the layers and give the measurement algorithm as raw data. We expect the method to be used in various fields of medicine. For example, by generalizing this method to measure the thickness and refractive index of retinal layers, the effect of different diseases on the amount and change of these quantities can be investigated.

Ethical Considerations

Not applicable.

Conflict of Interests

The authors declare no conflict of interest.

References

1. Fercher AF, Drexler W, Hitzenberger CK, Lasser T. Optical coherence tomography - principles and applications. *Rep Prog Phys*. 2003;66(2):239-303. doi:10.1088/0034-4885/66/2/204
2. Lu Y, Li Z, Zhang X, Ming B, Jia J, Wang R, et al. Retinal nerve fiber layer structure abnormalities in early Alzheimer's

disease: evidence in optical coherence tomography. *Neurosci Lett*. 2010;480(1):69-72. doi: 10.1016/j.neulet.2010.06.006

3. Akil H, Al-Sheikh M, Falavarjani KG, Francis B, Chopra V. Choroidal thickness and structural glaucoma parameters in glaucomatous, preperimetric glaucomatous, and healthy eyes using swept-source OCT. *Eur J Ophthalmol*. 2017;27(5):548-554. doi:10.5301/ejo.5000926
4. Ghasemi Falavarjani K, Iafe NA, Hubschman J-P, Tsui I, Sadda SR, Sarraf D. Optical coherence tomography angiography analysis of the foveal avascular zone and macular vessel density after anti-VEGF therapy in eyes with diabetic macular edema and retinal vein occlusion. *Invest Ophthalmol Vis Sci*. 2017;58(1):30-34. doi:10.1167/iovs.16-20579
5. Soltan Sanjari M, Parvaresh MM, Maleki A, Ghasemi Falavarjani KH, Bakhtiari P. Correlation between nerve fiber layer thickness on OCT and visual field in patients with optic atrophy. *Bina J Ophthalm*. 2008;13(3):331-335.
6. de Boer JF, Hitzenberger CK, Yasuno Y. Polarization sensitive optical coherence tomography - a review [Invited]. *Biomed Opt Express*. 2017;8(3):1838-1873. doi:10.1364/BOE.8.001838
7. Kolenderska S, Vanholsbeeck F, Kolenderski P. Quantum Optical Coherence Tomography using two-photon joint spectrum detection. *Opt Express*. 2020 ;28(20):29576-89. doi:10.1364/oe.399913
8. Jin J, Kim JW, Kang C-S, Kim J-A, Eom TB. Thickness and refractive index measurement of a silicon wafer based on an optical comb. *Opt Express*. 2010;18(17):18339. doi:10.1364/oe.18.018339
9. Na J, Choi HY, Choi ES, Lee C, Lee BH. Self-referenced spectral interferometry for simultaneous measurements of thickness and refractive index. *Appl Opt*. 2009;48(13):2461-2467. doi:10.1364/ao.48.002461
10. Leitgeb R, Hitzenberger C, Fercher A. Performance of fourier domain vs. time domain optical coherence tomography. *Opt Express*. 2003;11(8):889-894. doi:10.1364/oe.11.000889
11. Yun S, Tearney G, de Boer J, Iftimia N, Bouma B. High-speed optical frequency-domain imaging. *Opt Express*. 2003;11(22):2953-2963. doi:10.1364/oe.11.002953
12. Tahara S, Bezerra HG, Baibars M, Kyono H, Wang W, Pokras S, et al. In vitro validation of new Fourier-domain optical coherence tomography. *EuroIntervention*. 2011;6(7):875-882. doi:10.4244/EIJV6I7A149
13. Bouma BE, Yun S-H, Vakoc BJ, Suter MJ, Tearney GJ. Fourier-domain optical coherence tomography: recent advances toward clinical utility. *Curr Opin Biotechnol*. 2009;20(1):111-118. doi: 10.1016/j.copbio.2009.02.007
14. Yang Z, Tatham AJ, Zangwill LM, Weinreb RN, Zhang C, Medeiros FA. Diagnostic ability of retinal nerve fiber layer imaging by swept-source optical coherence tomography in glaucoma. *Am J Ophthalmol*. 2015;159(1):193-201. doi: 10.1016/j.ajo.2014.10.019
15. Potsaid B, Baumann B, Huang D, Barry S, Cable AE, Schuman JS, et al. Ultrahigh speed 1050nm swept source/Fourier domain OCT retinal and anterior segment imaging at 100,000 to 400,000 axial scans per second. *Opt Express*. 2010;18(19):20029-20048. doi:10.1364/OE.18.020029
16. Choma M, Sarunic M, Yang C, Izatt J. Sensitivity advantage of swept source and Fourier domain optical coherence tomography. *Opt Express*. 2003;11(18):2183-2189. doi:10.1364/oe.11.002183
17. Rajai P, Schriemer H, Amjadi A, Munger R. Simultaneous measurement of refractive index and thickness of multilayer systems using Fourier domain optical coherence tomography, part 2: implementation. *J Biomed Opt*. 2017;22(1):15003. doi: 10.1117/1.JBO.22.1.015003
18. Schmitt JM. Optical coherence tomography (OCT): a review. *IEEE J Sel Top Quantum Electron*. 1999;5(4):1205-1215. doi:10.1109/2944.796348
19. Zlokolica V, Jovanov L, Pižurica A, De Keyser P, Dhaenens F, Philips W. Wavelet-based denoising for 3D OCT images. Proc. SPIE 6696, Applications of Digital Image Processing XXX; 8 October 2007; San Diego, California, United States. doi: 10.1117/12.734286
20. Gelikonov GV, Gelikonov VM, Shilyagin PA. Linear wave-number spectrometer for spectral domain optical coherence tomography. Proc. SPIE 6847, Coherence Domain Optical Methods and Optical Coherence Tomography in Biomedicine XII; 18 February 2008; San Jose, California, United States. doi:10.1117/12.763541
21. Chan KKH, Tang S. High-speed spectral domain optical coherence tomography using non-uniform fast Fourier transform. *Biomed Opt Express*. 2010;1(5):1309-1319. doi:10.1364/BOE.1.001309
22. Leitgeb RA, Drexler W, Unterhuber A, Hermann B, Bajraszewski T, Le T, et al. Ultrahigh resolution Fourier domain optical coherence tomography. *Opt Express*. 2004;12(10):2156-2165. doi:10.1364/opex.12.002156
23. Dorrer, C, Belabas, N, Likforman, J, Joffre, M. Spectral resolution and sampling issues in Fourier-transform spectral interferometry. *J Opt Soc Am B*. 2000; 17(10):1795-1802. doi:10.1364/JOSAB.17.001795
24. Shin S, Sharma U, Tu H, Jung, W. Boppart S. Characterization and Analysis of Relative Intensity Noise in Broadband Optical Sources for Optical Coherence Tomography. *IEEE Photonics Technol Lett*. 2010; 22(14):1057-1059. doi:10.1109/LPT.2010.2050058
25. Moon S, Lee S, Chen Z. Reference spectrum extraction and fixed-pattern noise removal in optical coherence tomography. *Opt Express*. 2010; 18(24): 24395-404. doi:10.1364/OE.18.024395
26. Bashkansky M, Reintjes J. Statistics and reduction of speckle in optical coherence tomography. *Opt Lett*. 2000;25(8): 545-7. doi:10.1364/OL.25.000545
27. Li M, Idoughi R, Choudhury B, Heidrich, W. Statistical model for OCT image denoising. *Biomed Opt Express*. 2017; 8(9): 3903-17. doi:10.1364/BOE.8.003903
28. Wu Y, Tracey B, Natarajan P, Noonan J. James–Stein Type Center Pixel Weights for Non-Local Means Image Denoising. *IEEE Signal Process Lett*. 2013; 20(4): 411-414. doi:10.1109/LSP.2013.2247755
29. Leitgeb R, Hitzenberger C, Fercher A, Bajraszewski T. Phase-shifting algorithm to achieve high-speed long-depth-range probing by frequency-domain optical coherence tomography. *Optics Lett*. 2003; 28(22): 2201-4. doi:10.1364/OL.28.002201
30. Adhi M, Duker J. Optical coherence tomography – current and future applications. *Curr Opin Ophthalmol*. 2013;24(3): 213-221. doi: 10.1097/ICU.0b013e32835f8bf8
31. Gambichler T, Moussa G, Sand M, Sand D, Altmeyer P, Hoffmann K. Applications of optical coherence tomography in dermatology. *J Dermatol Sci*. 2005 40(2): 85-94. doi:10.1016/j.jdermsci.2005.07.006
32. Fujimoto J, Drexler W, Schuman J, Hitzenberger, C. Optical Coherence Tomography (OCT) in Ophthalmology: Introduction. *Opt Express*. 2009;17(5): 3978-9. doi:10.1364/oe.17.003978